Appl Phys A (2013) 110:23–28
DOI 10.1007/s00339-012-7330-7

Applied Physics A
Materials Science & Processing

RAPID COMMUNICATION

Use of distributed Bragg reflectors to enhance Fabry–Pérot lasing in vertically aligned ZnO nanowires

Jieying Kong · Sheng Chu · Jian Huang · Mario Olmedo · Weihang Zhou · Long Zhang · Zhanghai Chen · Jianlin Liu

Received: 17 August 2012 / Accepted: 10 October 2012 / Published online: 17 October 2012

Abstract An optically pumped ZnO nanowire laser with a 10-period SiO_2/SiN_x distributed Bragg reflector (DBR) was demonstrated. Stimulated emissions with equally distributed Fabry–Pérot lasing modes were observed at pumping powers larger than 121 kW/cm^2. This result, when compared to nanowires of the same length and without a DBR structure, shows that a lower threshold of pumping power, higher quality factor, and larger cavity finesse can be achieved due to the high reflectivity of the DBR in the designed wavelength range. A coexistence of stimulated and spontaneous emissions was also observed above threshold and was attributed to partially confined waveguide modes in nanowires with diameters smaller than 100 nm.

1 Introduction

Ultraviolet (UV) semiconductor diode lasers are widely used in information processing, data storage, and biology. However, their applications have been limited by large size and high cost. Semiconductor nanostructures are thereby attracting tremendous attention for the next-generation nanolasers and waveguides. ZnO can be synthesized at low cost, and it has a direct wide band gap of around 3.30 eV, which makes it one of the most promising candidates to realize UV lasing at room temperature. Random lasing was detected in ZnO nanopowders [1–3], nanowires [4–7], polycrystalline films [8–10] under optical excitation. However, since the random emissions from disordered ZnO material are directionless and mode varying [11, 12], random lasing faces potential limitations in traditional laser applications such as communication and media. On the other hand, it is highly desirable to achieve Fabry–Pérot lasing from ZnO nanowires because the naturally formed flat ends of nanowires avoid the difficulty of cleaving smooth facets in order to sustain lasing, leading to coherent beams with reliable modes. A great deal of effort has already been made in establishing optically pumped ZnO Fabry–Pérot type lasing [13–16], in both single nanowires and large-scale vertically aligned nanowire bundles [17, 18]. Recently, our group has also demonstrated electrically pumped Fabry–Pérot lasing in vertically aligned ZnO nanowires grown with a catalyst free ZnO seed layer on sapphire substrate [7]. Nevertheless, all of these results showed a relatively high threshold power due to a large cavity loss at the ZnO/sapphire and/or ZnO/air interfaces. It is possible to further engineer the end mirrors of nanowire cavity by increasing their reflectivities and achieve lower threshold pumping power.

DBR structures have been widely adopted in the vertical cavity semiconductor laser diode fields to reduce the threshold pumping density and enhance laser performance. The 50 % reduction of threshold power was reported by employing DBR mirrors at both ends of the cavity [19]. DBR was already attempted in GaN nanowires to achieve polariton lasing [20], although it was rarely reported in nanowires made of other materials such as ZnO. This may originate from the difficulty of precise deposition of desirable multilayer DBR on the ends of the ZnO nanowires. In this paper, we report a solution by direct growth of vertically aligned ZnO nanowires on SiO_2/SiN_x DBR films. There are two advantages to use SiO_2/SiN_x DBR to enhance the performance

J. Kong · S. Chu · J. Huang · M. Olmedo · J. Liu (✉)
Quantum Structures Laboratory, Department of Electrical Engineering, University of California, Riverside, CA 92521, USA
e-mail: jianlin@ee.ucr.edu

W. Zhou · L. Zhang · Z. Chen
Laboratory of Advanced Materials, Department of Physics, Fudan University, Shanghai 200433, China

of ZnO nanowire lasers. First, the contrast of refractive index between SiO_2 and SiN_x is relatively large at working wavelength in UV. The number of dielectric pairs required to achieve high reflectivity is therefore reduced [21]. Second, SiO_2 and SiN_x are insulators, which minimize the absorption at ZnO band edge energy. The thicknesses of the alternate layers of the DBR were designed to confine the near-band-edge emission of ZnO nanowires. With the presence of the DBR structures, we carried out optical pumping of vertically aligned ZnO nanowires and demonstrated that the threshold of nanowire lasing is reduced and cavity performance is enhanced.

2 Material and methods

SiO_2/SiN_x DBR structures were grown on c-plane sapphire substrates in plasma enhanced chemical vapor deposition (PECVD). Standard gaseous processes of SiO_2 and SiN_x were used. The plasma power was 25 watts at a source radio frequency of 13.56 MHz. The substrate temperature was 300 °C during the growth. After the DBR was fabricated, the sample was transferred to a plasma assisted molecular beam epitaxy (MBE) system. The MBE process started with a few nanometers of ZnO buffer layer growth at 350 °C, followed by one micron ZnO layer growth at 550 °C. The polycrystalline ZnO thin film consists of closely packed column structures. The *c*-axis of ZnO grain is highly directional, which is perpendicular to the substrate plane. This polycrystalline layer acts as seed layer for the subsequent vertically aligned ZnO nanowire growth. ZnO nanowires were then grown on top of the column structured ZnO layer by chemical vapor deposition (CVD). The CVD is a horizontal quartz tube furnace system (Thermal Scientific Inc.). Zinc powder (99.999 % Sigma Aldrich) in a glass bottle was placed in the center of the tube, with the ZnO sample placed about 8 cm downstream from it. A flow of 606 sccm of nitrogen was passed continuously through the furnace. The source and sample were then heated to 515 °C at a ramp rate of 30 °C per minute. Once the temperature was reached, 188 sccm flow of a mixture of argon/oxygen (99.5:0.5 % by volume) was introduced to the tube for ZnO nanowire growth for 15 minutes.

3 Results and discussion

Reflectance of the DBR structures was measured using a Shumadzu UV-3101PC spectrometer. The reflectance spectrum was converted by a transmission measurement under normal incidence from 250 nm to 800 nm, with the assumption that the absorption in the measurement is zero. The morphology of the DBR structures and nanowires was characterized using scanning electron microscopy (SEM) and transmission electron microscopy (TEM). Regular photoluminescence (PL) spectrum was acquired from the excitation by a 325 nm He–Cd laser. High-intensity optical pumping was carried out using the frequency-tripled output (355 nm) of a Nd:YAG pulse laser with a repetition rate of 10 Hz and 3 ns pulse duration. The excitation laser beam was focused to form an excitation spot of 14 μm in diameter on the nanowires. A charge coupled device (CCD camera) with a choice of high resolution was used to detect the emission, which was coupled into an optical fiber. The data were collected using a computer.

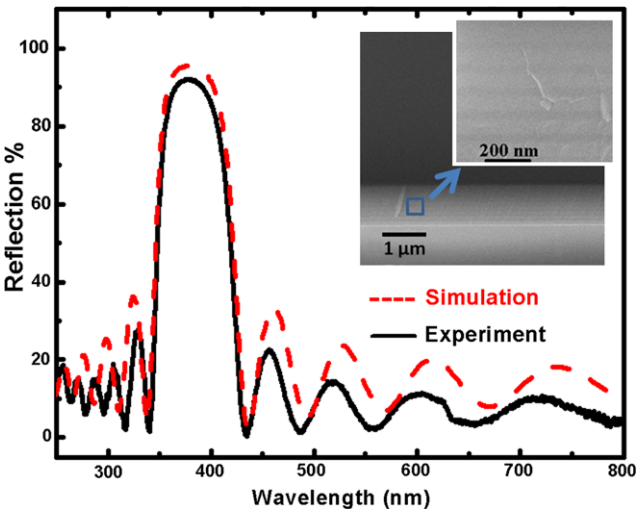

Fig. 1 Experimental and simulated reflection spectra of the DBR structure from 250 nm to 800 nm. The *inset* shows cross sectional SEM image of 10-period SiO_2/SiN_x dielectric DBR structure

The SEM image shown in the inset of Fig. 1 is the cross section of the DBR layers on top of the sapphire substrate. As seen from the image, the interfaces between SiO_2 and SiN_x are fairly smooth, hence the interface scattering between the layers is minimized. Total 10 pairs of SiO_2 and SiN_x layers of 60.9 nm and 48.7 nm, respectively, are observed. The thicknesses match with $\lambda/4$ requirement of SiO_2 and SiN_x layers, with a consideration of the refractive index of 1.56, and 1.95, respectively. Figure 1 shows reflection spectra of this DBR structure from the measurement and simulation based on transfer matrix method [21]. It is evident that both calculated and measured results are in good agreement, indicating that the DBR gives desirable optical quality and the reflectivity at 380–390 nm reaches 95 %.

Figure 2(a) and (b) show top-view and side-view SEM images of the nanowire sample, respectively. The as grown ZnO nanowires follow the *c*-axis of the ZnO grains of the seed film, and are vertically aligned. The lengths of nanowires range from 10 μm to 11 μm, while the diameters of nanowires range from 50 nm to 300 nm, among which 95 % of the nanowires are larger than 100 nm, and 75 % of nanowires are larger than 200 nm. Figure 2(c) shows a

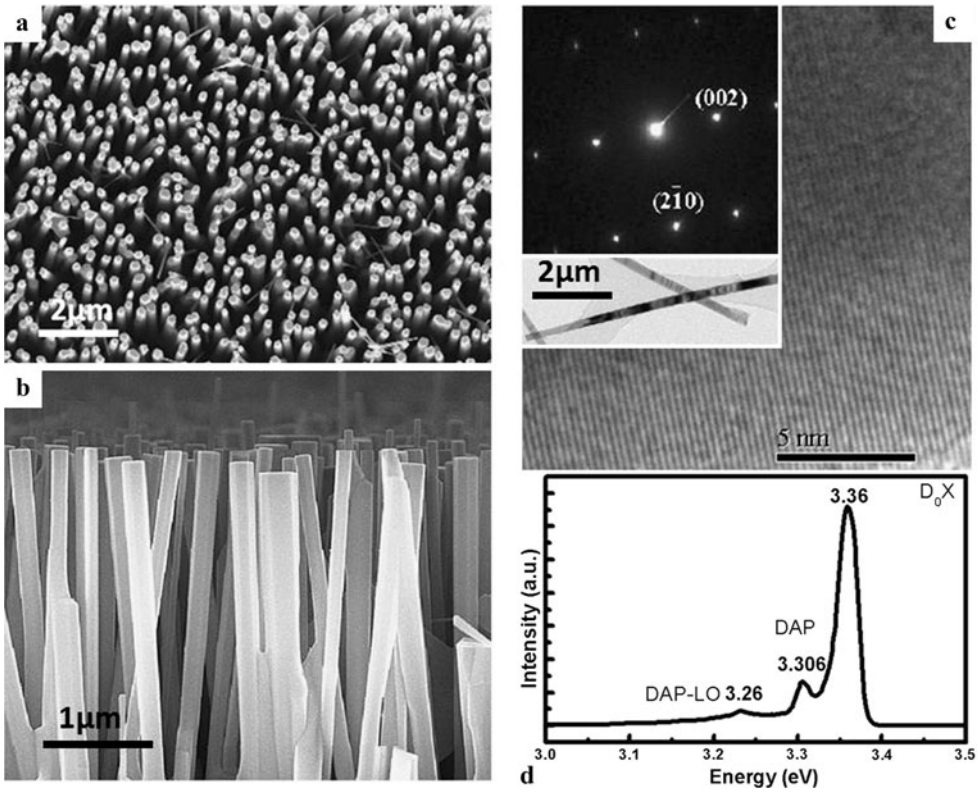

Fig. 2 (**a**) Top-view SEM image of the vertically aligned nanowires grown with a ZnO seed layer on DBR structure. (**b**) Side-view SEM image of the vertically aligned nanowires. (**c**) High-resolution TEM image of one nanowire. *Inset* shows a lower magnification TEM image of nanowires and corresponding electron diffraction pattern. (**d**) PL spectrum of the sample excited by 325 nm excitation laser at 10 K

high-resolution TEM image of a typical single nanowire, revealing a single-crystal wurtzite structure. A lower magnification TEM image of the nanowire is shown as the bottom inset of Fig. 2(c) and a selected area electron diffraction pattern confirms that the nanowire grows along *c*-axis, as shown in the top inset of Fig. 2(c). Figure 2(d) shows a PL spectrum of the nanowires measured at 10 K. There are three peaks, which are related to donor-bound exciton (D_0X), donor-acceptor pair recombination and its phonon replica, indicating good optical quality.

Figure 3(a) shows the evolution of the luminescence spectra at the excitation intensity ranging from 45 kW/cm^2 to 500 kW/cm^2. At low excitation power, a broad emission with peak energy at 3.23 eV is evident, which corresponds to ZnO near-band-edge spontaneous emission. As the excitation power increases, several sharp peaks with full width at half maximum (FWHM) of about 3 meV start to shoot up, indicating an onset of lasing emission. For comparison, the emission of the same length nanowires without a bottom DBR structure as a function of pumping power from 45 kW/cm^2 to 500 kW/cm^2 is shown in the inset of Fig. 3(a). *Y*-axis in this plot is in log scale to show clearly individual modes in the emission, which are marked by red arrows. Although one mode at around 388 nm dominates compared with other modes, it is not considered as a single mode laser because the intensity of other modes increase significantly with pumping power higher than 500 kW/cm^2 (not shown here). Note that the lasing modes are distributed on a broad spontaneous emission, which is from the body emission of the non-lasing nanowires [22]. As seen in Fig. 2(a) and (b), the nanowires have size variation, it is possible that some nanowires within excited area lase, while the others remain spontaneous emissions. Due to strong spontaneous emission, the onset of lasing is difficult to observe from excitation power dependant intensity evolution. To separate the spontaneous and stimulated emissions, Gaussian fitting was carried out for the spectra of all excitation powers. Figure 3(b) shows the fitted result of the emission at 450 kW/cm^2, which is divided into 10 peaks consisting of two broad emission peaks and eight sharp peaks with even spacing. Figure 3(c) and 3(d) show the integrated intensity vs. excitation power for the reference nanowire sample without DBR structure and the nanowire sample with DBR structure, respectively. The spontaneous emissions follow a sublinear evolution and the stimulated emissions show superlinear characteristic with clear onset lasing threshold. The superlinear characteristic suggests that excitonic process instead of electron-hole plasma process plays dominant role at this pumping level [28]. The power-dependent intensity can be well described by power law $I_{(\mathrm{out})} \sim I_{(\mathrm{in})}^{P}$, with $p = 3.03$ for reference nanowires and $p = 3.08$ for nanowires grown on DBR. Larger exponential coefficient p means higher 'slope' efficiency in log scale plot. The two solid straight lines are drawn to guide eyes, indicating a reduction of the threshold power by 20 % from 150 kW/cm^2 to 121 kW/cm^2 for the samples without and with DBR,

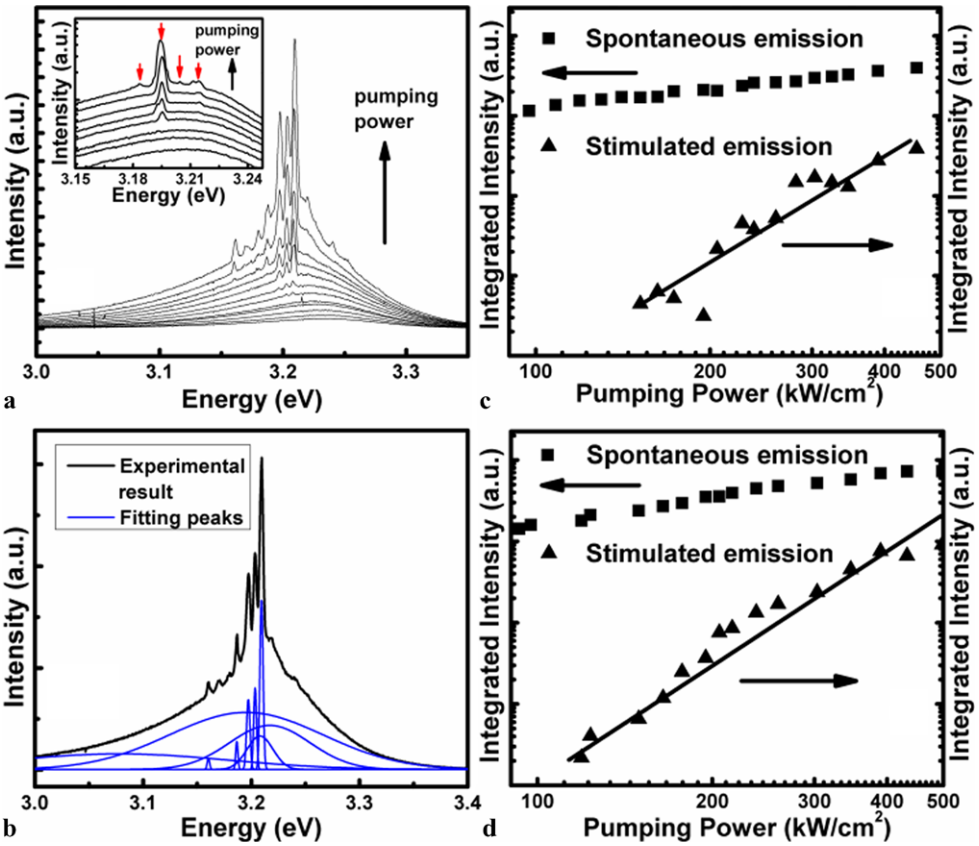

Fig. 3 (**a**) PL spectra of the vertically aligned nanowires with optical pumping power from 45 kW/cm^2 to 500 kW/cm^2. The *inset* shows the optically pumped PL spectra from a reference ZnO nanowire sample with the same length and no DBR underneath. (**b**) Emission of ZnO nanowires on DBR structure at pumping power of 450 kW/cm^2. The spectrum is fitted with multiple Gaussian peaks. (**c**) Integrated intensity of spontaneous and stimulated emissions under different pumping power from the sample grown without DBR. (**d**) Integrated intensity of spontaneous and stimulated emissions under different pumping power from the sample grown on DBR structure

respectively. This 20 % reduction of threshold can be explained by considering the threshold expression in a Fabry–Pérot resonator, which is written as $g_{\text{th}} = \gamma + \frac{1}{2L}\ln(\frac{1}{R_1 \times R_2})$ [23], where γ is the transition loss, L is the length of the nanowire, and R_1, R_2 denote the reflectivity at each end of the cavity. With the DBR structure as the bottom reflector, the reflectivity increases from 3 % (ZnO/sapphire interface) to 95 %, leading to the lower threshold pumping power. It should be noted that threshold powers of ZnO nanowire lasers vary from 40 kW/cm^2 to 350 kW/cm^2 as seen from literature so far [4, 7, 24]. The present threshold powers are not lower than those lowest reported values because threshold powers of nanowire laser not only depend on the reflectivities of the end mirrors but also depend on nanowire synthesis processes (relating to γ) and nanowire lengths (L). Since the nanowires in the present study were synthesized using the same process recipe and have the same lengths, the difference of the threshold power is mainly caused by introducing DBR structure. In addition, 20 % reduction is fairly reasonable considering that only one end of the cavity employs DBR structure.

Figure 4(a) shows lasing spectrum at the pumping power of 500 kW/cm^2 in comparison with the calculated Fabry–Pérot cavity modes confined in a Gaussian distributed peak with center energy at 3.20 eV. The mode distribution was obtained by using Airy function $A = [1 + F\sin^2(\omega/2)]^{-1}$, where ω is circular frequency, which can be transformed from energy, and F is cavity finesse, which can be written as $F = \frac{4(R_1R_2)^{1/2}}{[1-(R_1R_2)^{1/2}]^2}$. For the nanowires grown on DBR structure $R_1 = 95$ %, $R_2 = 18$ %, F is calculated to be 4.8, which is greatly enhanced from 0.34 for the nanowires grown without DBR on sapphire substrate. Considering that the average length of the nanowires is 10 nm, and the refractive index of ZnO at band edge follows the expression $n' = n - \lambda(dn/d\lambda)$, where $n = 2.5$ is the refractive index of ZnO below band edge and $dn/d\lambda = -0.015$ nm^{-1} denotes the dispersion relation for the refractive index [25], the simulated mode distribution is in close agreement with the observed experimental result, i.e., evenly distributed mode spacing of about 1 nm (6 meV). The peak positions and mode spacing stay the same under different excitations as well, which is a strong evidence of Fabry–Pérot type resonance [26].

Figure 4(b) shows the statistic distribution of experimental quality factor (Q) as a function of pumping power above thresholds for the two samples with and without DBR structure, respectively. The dashed lines denote average Q factors for the two samples. The Q factor increases from 865 for the sample without DBR to 1067 for the sample with DBR, indicating higher performance of the cavity thanks to the larger reflectivity from DBR. With increased excitation

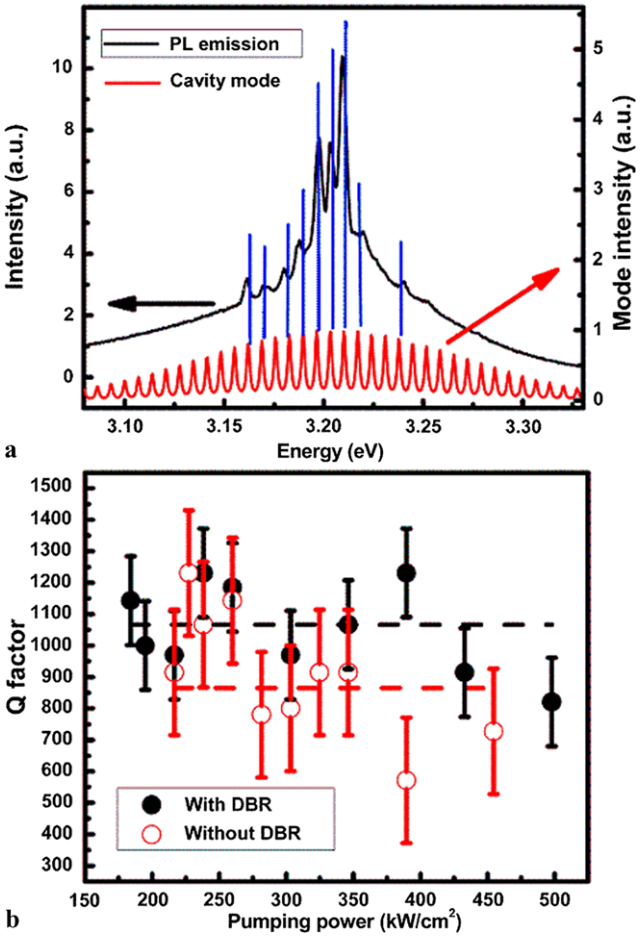

Fig. 4 (**a**) PL spectrum at excitation power of 500 kW/cm^2, with the calculated mode distribution at different energy. (**b**) Quality factor Q distribution from the two nanowire laser samples with and without DBR structure

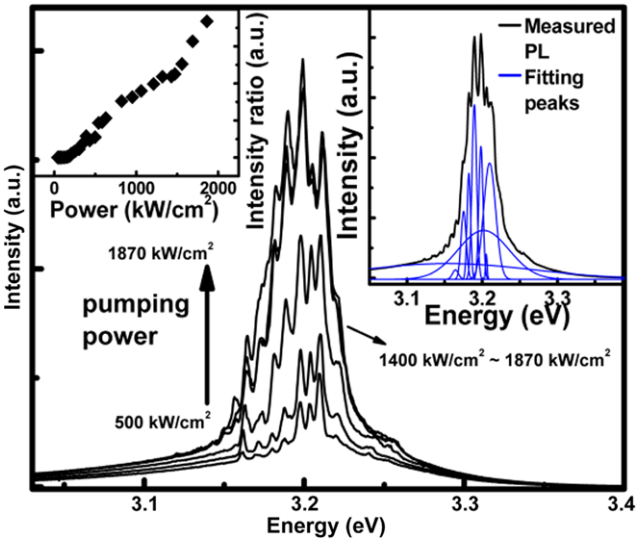

Fig. 5 PL spectra of the vertically aligned nanowire laser sample with DBR at the pumping power from 500 kW/cm^2 to 1870 kW/cm^2. The *top right inset* shows a typical emission at 1870 kW/cm^2, with multiple peaks fitted by Gaussian distribution. The *top left inset* shows the intensity ratio between stimulated emission and spontaneous emission above threshold

power, the Q factors appear to decrease owing to the heat induced FWHM expansion.

Figure 5 shows lasing spectra at higher excitation power between 500 and 1870 kW/cm^2. Stronger lasing modes superimposing on the broad near-band-edge spontaneous emission peak are evident. The right top inset is Gaussian fitted result of the emission with excitation power at 1870 kW/cm^2. The two broad peaks are spontaneous emissions, indicating that even at these very large pumping powers, there is coexistence of spontaneous and stimulated emissions [27]. This is mainly due to the statistical results of lasing from multiple nanowires with different sizes. Note that the excitation laser beam size is about 14 μm in diameter, the excitation area would contain hundreds of nanowires with size variation from 50 nm to 300 nm in diameter. The emissions from these nanowires have different modes reliability. A rough calculation shows that the fractional mode power within the core of the waveguide of 200 nm in diameter is about 90 %. However, less than 25 % of the field intensity is present inside the wire with diameter less than 100 nm [28].

Consequently, highly efficient confinement of light only occurs in the nanowires with diameters of 200 nm or larger. For the nanowires with small diameters, body emission will be dominant instead of resonant formation, leaving a broad emission peak even with very high pumping power above threshold. The intensity ratio between stimulated emission and spontaneous emission increases with the increase of excitation power (shown in the left top inset of Fig. 5), which means that the stimulated emission intensity grows faster than spontaneous emission. The power saturation was observed above 1400 kW/cm^2, which is due to the transient thermal population and the participation of non-radiative recombination [28]. The lasing modes at high excitation range are also stable, though there is a slight blueshift, compared with those at excitation powers less than 500 kW/cm^2. The blueshift is mainly due to temperature induced refractive index variation [29].

4 Summary

We grew a 10-period DBR structure with designed thicknesses of the alternative layers made from SiO_2 and SiN_x. The reflectivity at 380–390 nm reaches 95 %. Vertically aligned ZnO nanowires were achieved by CVD growth, on a ZnO polycrystalline seed layer deposited on DBR by MBE. Fabry–Pérot type lasing was observed with optical pumping and a 20 % lower threshold excitation power was achieved due to the lower cavity loss with the DBR structure. The cavity finesses is improved from 0.34 to 4.8 with one end DBR

structure, hence the FWHM of lasing mode is reduced from 4 meV to 3 meV. The competition between spontaneous and stimulated emission was further studied at higher pumping power. The non-extinct spontaneous emission is due to fractional confinement of waveguide modes in small nanowires less than 100 nm in diameter. The present DBR on sapphire technology can be readily transferred on Si or even glass substrates, further lowering the cost. The achievement of lower threshold pumping power with DBR structure paves a way for future development of low-threshold ZnO nanowire laser diodes.

Acknowledgements This work is supported by NSF (Grant No. ECCS-0900978). The authors thank Krassimir N. Bozhilov for assistance in TEM imaging.

References

1. T. Nakamura, B.P. Tiwari, S. Adachi, Appl. Phys. Lett. **99**, 231105 (2011)
2. H. Cao, J.Y. Xu, D.Z. Zhang, S.-H. Chang, S.T. Ho, E.W. Seelig, X. Liu, R.P.H. Chang, Phys. Rev. Lett. **84**, 5584 (2000)
3. R.K. Thareja, A. Mitra, Appl. Phys. B **71**, 181 (2000)
4. M.H. Huang, S. Mao, H. Feick, H. Yan, Y. Wu, H. Kind, E. Weber, R. Russo, P. Yang, Science **292**, 1897 (2001)
5. P. Yang, H. Yan, S. Mao, R. Russo, J. Johnson, R. Saykally, N. Morris, J. Pham, R. He, H.J. Choi, Adv. Funct. Mater. **12**, 323 (2002)
6. R. Yan, D. Gargas, P. Yang, Nat. Photonics **3**, 569 (2009)
7. S. Chu, G. Wang, W. Zhou, Y. Lin, L. Chernyak, J. Zhao, J. Kong, L. Li, J. Ren, J. Liu, Nat. Nanotechnol. **6**, 506 (2011)
8. Z.K. Tang, G.K.L. Wong, P. Yu, M. Kawasaki, A. Ohtomo, H. Koinuma, Y. Segawa, Appl. Phys. Lett. **72**, 3270 (1998)
9. S. Cho, J. Ma, Y. Kim, Y. Sun, K.L. Wong, J.B. Ketterson, Appl. Phys. Lett. **75**, 2761 (1999)
10. S. Chu, M. Olmedo, Z. Yang, J. Kong, J. Liu, Appl. Phys. Lett. **93**, 181106 (2008)
11. C. Yuen, S.F. Yu, S.P. Leong, H.Y. Yang, S.P. Law, N.S. Chen, H.H. Hng, Appl. Phys. Lett. **86**, 031112 (2005)
12. H. Cao, Y.G. Zhao, S.T. Ho, E.W. Seelig, Q.H. Wang, R.P.H. Chang, Phys. Rev. Lett. **82**, 2278 (1999)
13. H. Yan, R. He, J.C. Johnson, M. Law, R.J. Saykally, P. Yang, J. Am. Chem. Soc. **125**, 4728 (2003)
14. D.J. Gargas, M.E. Toimil-Molares, P. Yang, J. Am. Chem. Soc. **131**, 2125 (2009)
15. J. Fallert, R.J.B. Dietz, H. Zhou, J. Sartor, C. Klingshirn, H. Kalt, Phys. Status Solidi C **2**, 449 (2009)
16. L.K. Vugt, S. Ruhle, D. Vanmaekelbergh, Nano Lett. **6**, 2707 (2006)
17. Y. Wei, W. Wu, R. Guo, D. Yuan, S. Das, Z. Wang, Nano Lett. **10**, 3414 (2010)
18. S. Zhang, Y. Shen, H. Fang, S. Xu, J. Song, Z. Wang, J. Mater. Chem. **20**, 10606 (2010)
19. T. Saito, M. Kumagai, H. Wang, T. Tawara, T. Nishida, T. Akasaka, N. Kobyashi, Appl. Phys. Lett. **82**, 4426 (2003)
20. A. Das, J. Heo, M. Jankowski, W. Guo, L. Zhang, H. Deng, P. Bhattacharya, Phys. Rev. Lett. **107**, 066405 (2011)
21. J. Carroll, J. Whiteaway, D. Plumb, *Distributed Feedback Semiconductor Lasers* (Redwood Books, Trowbridge, 1998)
22. D. O'Carroll, I. Lieberwirth, G. Redmond, Nat. Nanotechnol. **2**, 180 (2007)
23. A.B. Djurisic, Y.H. Leung, Small **2**, 944 (2006)
24. K. Bando, T. Sawabe, K. Asaka, Y. Masumoto, J. Lumin. **108**, 385 (2004)
25. V.V. Ursaki, V.V. Zalamai, I.M. Tiginyanu, A. Burlacu, E.V. Rusu, C. Klingshirn, Appl. Phys. Lett. **95**, 171101 (2009)
26. S. Ruhle, L.K. van Vugt, H.Y. Li, N.A. Keizer, L. Kuipers, D. Vanmaekelbergh, Nano Lett. **8**, 119 (2008)
27. L. Chen, E. Towe, Appl. Phys. Lett. **89**, 053125 (2006)
28. J.C. Johnson, H. Yan, P. Yang, R.J. Saykally, J. Phys. Chem. B **107**, 8816 (2003)
29. V.S. Park, J.R. Schneider, J. Appl. Phys. **39**, 3049 (1968)